Electronic properties of *β*-TaON and its surfaces for solar water splitting

Habib Ullah[a,*], Asif A. Tahir[a,*], Salma Bibi[b], Tapas K. Mallick[a], Smagul Zh. Karazhanov[c]

[a] *Environment and Sustainability Institute (ESI), University of Exeter, Penryn Campus, Penryn, Cornwall TR10 9FE, UK*
[b] *National Centre of Excellence in Physical Chemistry, University of Peshawar, 25120 Peshawar, Pakistan*
[c] *Department for Solar Energy, Institute for Energy Technology, 2027 Kjeller, Norway*

ARTICLE INFO

ABSTRACT

Recently, oxynitrides materials such as *β*-TaON has been using as a photoanode material in the field of photo-catalysis and is found to be promising due to its suitable band gap and charge carrier mobility. Computational study of the crystalline *β*-TaON in the form of primitive unit cell, supercell and its N, Ta, and O terminated surfaces are carried out with the help of periodic density functional theory (DFT). Optical and electronic properties of all these different species are simulated, which predict TaON as the best candidate for photo-catalytic water splitting contrast to their Ta_2O_5 and Ta_3N_5 counterparts. The calculated bandgap, valence band, and conduction band edge positions predict that *β*-TaON should be an efficient photoanodic material. The va-lence band is made up of N 2p orbitals with a minor contribution from O 2p, while the conduction band is made up of Ta 5d. Turning to thin films, the valence band maximum; VBM (-6.4 eV vs. vacuum) and the conduction band minimum; CBM (-3.3 eV vs. vacuum) of (010)-O terminated surface are respectively well below and above the redox potentials of water as required for photocatalysis. Charge carriers have smaller effective masses than in the (001)-N terminated film (VBM -5.8 and CBM -3.7 eV vs. vacuum). However, due to wide band gap (3.0 eV) of (010)-O terminated surface, it cannot absorb visible wavelengths. On the other hand, the (001)-N terminated TaON thin film has a smaller band gap in the visible region (2.1 eV) but the bands are not aligned to the redox potential of water. Possibly a mixed phase material would produce an efficient photoanode for solar water splitting, where one phase performs the oxidation and the other reduction.

1. Introduction

Solar fuel (H_2) is generated by photocatalytic water splitting when sunlight irradiates on a suitable semiconducting material [1–3]. Such catalytic materials should be robust, corrosion resistive and efficient light harvesters [4]. Since the discovery of photocatalytic water split-ting by Honda and Fujishima [5], the use of many semiconducting materials and transition metal oxides in particular have been explored in the search for photon-energy conversion. Photocatalysts drive the dissociation of water by coupling this to the photo-excitation of elec-trons [6,7], and an ideal material must have a narrow band gap cor-responding to the absorption of visible light and band edge positioned appropriately, so, that the valence band maximum (VBM) is more ne-gative than the redox potential for oxidation of water (-5.7 eV vs. vacuum) and the conduction band minimum (CBM) more positive than the redox potential for reduction of water (-4.5 eV vs. vacuum). Some semiconductors have band edges positioned appropriately aligned with the redox potentials of water but they are either unstable or have large band gaps. Others have narrow band gaps but one of the band edges

(VBM or CBM) is aligned unsuitably (Scheme 1) [8].

Oxynitrides have recently attracted much attention [9–15] while transition metal oxide semiconductors are also suitable candidates as photocatalysts for storable fuels because of their low cost, nontoxicity, abundance, and high corrosion resistance [16–18]. They have low ef-ficiencies due to their poor carrier conductivity and generally have large bandgaps [19]. To reduce the band gap, many methods have been tried, including defect formation and doping by cations and anion [20,21]. Incorporation of N is also a promising way as the N 2p states are energetically shallower than the deeper O 2p orbitals [22]. Gen-erally, the CBM of a transition metal oxynitride is mainly formed from the empty metal orbitals while the VBM of oxynitrides are shifted to more negative energy by N 2p mixed states [23,24]. Thus the band gaps of oxynitrides can be narrower than those of the corresponding metal oxides [21,22]. Recently, Cui et al. and Respinis et al. have compre-hensively investigated the electronic structures and photocatalytic ac-tivities of tantalum-based compounds such as Ta_2O_5, TaON, Ta_3N_5, and shown that the TaON exhibit visible-light photocatalytic activity since they have smaller band gaps compared to common oxides [25,26].
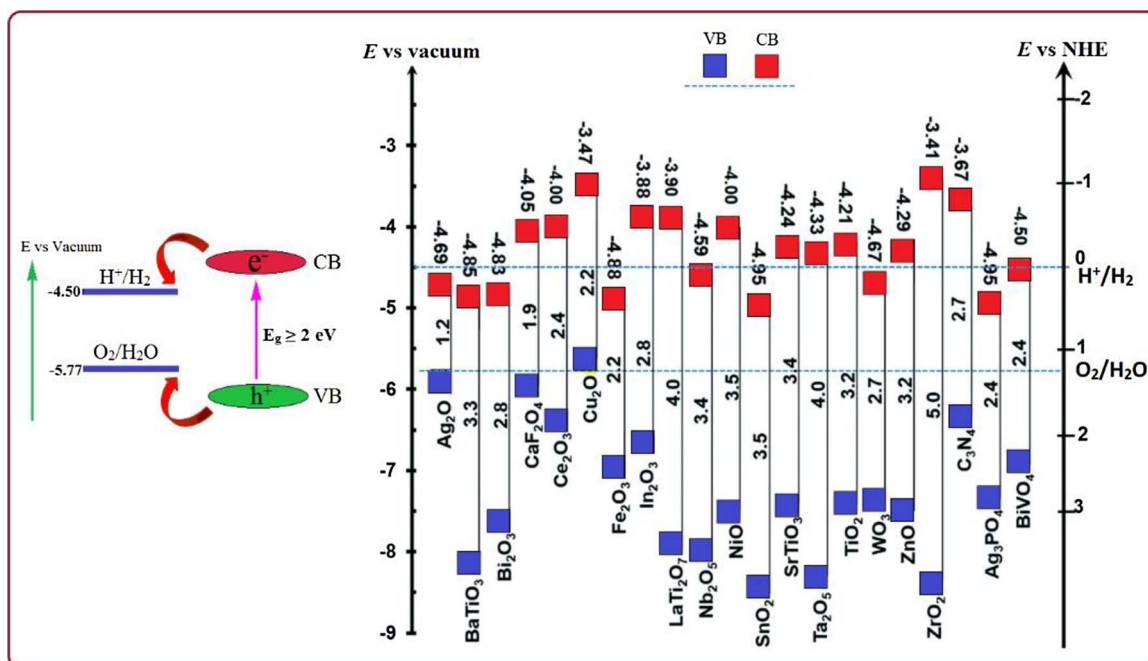
Scheme 1. VBM and CBM positions of selected semiconductors at pH 0 with respect to vacuum and normal hydrogen electrode (NHE) levels (in unit of eV): The redox potential of water is shown in blue solid and doted lines.

Tantalum oxynitride (TaON) is one promising material as a photo-anode for solar water splitting but works under external applied bias. Moreover, it has been reported that suitable energy of valence and conduction band edges of TaON make it an electrode material for both water oxidation and reduction, and a narrow band gap of ∼2.4 eV allows absorption of visible light [16,27,28]. However, the photocatalytic activity of TaON is still limited, due to self-deactivation upon irradiation, conversion of TaON to Ta_2O_5, high exciton binding energy, and ultra-fast electron-hole recombination [27,29].

In this work, we employ first principle periodic density functional theory (DFT) simulations to examine the optical and electronic properties of β-TaON. TaON exists in three different polymorphs, a hexagonal α-TaON phase, monoclinic β-TaON, and a metastable γ-TaON phase [30,31]. The α-TaON polymorph, with 9-fold metal coordination, adopts the cotunnite structure [32]. Another TaON polymorph, γ-TaON, having a monoclinic crystal structure [30,33]. The archetypal oxynitride of tantalum, β-TaON has the baddeleyite structure in which the Ta coordination number is seven and an ordered O/N anionic sub lattice. β-TaON is thermodynamically the most stable (up to 800 °C) polymorph of TaON [34]. We consider bulk β-TaON and its six different slabs such as (001)-N, (010)-N, (001)-O, (010)-O, (001)-Ta, and (010)-Ta. Among all these slabs, the (010)-O and (001)-N terminated surfaces were found to be suitable ultra-thin films for solar water splitting applications. Finally, we examined water adsorption on these selected films because of their potential as water splitting photocatalyst.

2. Computational details

First principle DFT calculations were performed using Quantum Espresso [35] and QuantumWise-ATK [36] and the results are visualized using Virtual NanoLab Version 2017.1 [37]. β-TaON (hereafter denoted as TaON) has a monoclinic structure in the $P\,2_1/C$ space group [33]. The primitive unit cell contains 12 atoms and the initial crystal structure parameters in our calculations are taken from experimental data (Table S1) [38]. After optimizing the lattice parameters of the unit cell, a (2 × 2 × 2) supercell was constructed. (010) and (001) slabs for each O, N, and Ta atoms were built by cleaving appropriately the 2 × 2 supercell of TaON. For the slab model calculations of surface energies

and band edge positions, the thickness of the slabs were four primitive unit cells of TaON (5 Å thick, having 48 atoms), to ensure that the centre of the slab can be regarded as the bulk phase. Lattice parameters of all these stoichiometric slabs are given in Table S2 of the Supporting Information. A vacuum space of about 15 Å was incorporated between slabs, to eliminate the fictitious interaction between periodically repeating slabs. Generalized gradient approximation (GGA) with the Perdew-Burke-Ernzerhof (PBE) exchange-correlation functional and double Zeta Polarized (DZP) basis set is used for the structural and energy optimization due to its superiority over hybrid pseudopotentials [39]. Moreover, linear combination of atomic orbitals (LCAO) method is used for Ta, N, H, and O atoms [40]. A 9 × 9 × 9 Monkhorst-Pack k-grid and energy cutoff of 900 eV is used for the unit cell and supercell of TaON while a 9 × 9 × 1 k-point mesh is used for the slabs. A complicated issue is the choice of appropriate basis and exchange-correlation function in DFT. Both the local density approximation (LDA) and GGA generally suffer from a large underestimation of bandgaps, while, meta-GGA can produce accurate values [41,42]. Hence meta-GGA is used for the band gap simulations in the Truhlar Blaha exchange functional and the correlation functional of Perdew-Zunger (LDA) in the form of TB09LDA [42]. Density of states (DOS), partial density of states (PDOS), band structure and effective masses of photogenerated electrons and holes are calculated. The DFT occupied and unoccupied DOS are considered as the VB and CB edges, respectively; separated by an energy equal to the known optical band gap [43]. The absorption spectra are calculated from the dielectric constant and plotted as a function of the wavelength, using TB09LDA [42].

3. Results and discussion

3.1. Selection of slabs and theoretical method

Geometries of unit cell, supercell, and slabs are optimized prior to their electronic and optical properties simulation. The crystal structure of unit cell is compared with the available crystallographic parameters of TaON (Fig. 1 and Table S1). PBE/GGA reproduces the experimental data accordingly as can be seen from Table S1 [38]. Moreover, we have also simulated the per atom cohesive formation energy of Ta, O, and N
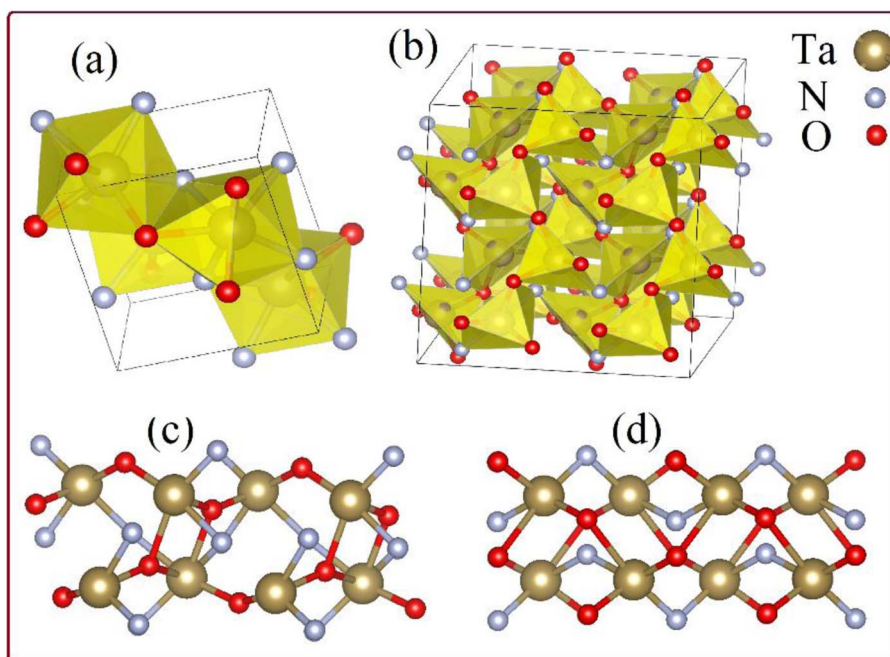
Fig. 1. Optimized Crystal structure of unit cell (a), supercell (b), N-terminated (c), and O-terminated (d) slab of TaON.

which has validated our computational method (see Table S3). The cohesive formation energy of Ta, at GGA/PBE using DZP basis set is 10 eV/atom and has nice correlation with the experimental reported one (8.10 eV/atom) [44]. The simulated cohesive formation energy of O and N are 3.7 and 3.1 eV/atom while their experimental values are 2.60 and 4.91 eV/atom, respectively [44].

The calculated band edge, band gap and formation energy of these six different slabs are listed in Table S4, where the (010)-O and (001)-N terminated surfaces have suitable VB, CB, band gap and formation energies, to be used for water splitting applications. Some of these slabs are either unstable or have inappropriately VB and CB positions, as can be seen from Table S4. So, we restrict our simulations to these two phases of TaON which are given in Fig. 1. These surfaces are constructed without any dipole; means the top and bottom layers were kept similar. The surface formation energy of these slabs was calculated using Eq. (1),

$$E_{surf} = \frac{1}{2A}(E_{slab} - NE_{bulk}) \tag{1}$$

where E_{slab} is the total energy of the slab, E_{bulk} is the energy per atom of the bulk, N denotes the number of atoms in the surface slab, and A is the cross-sectional area of the surface slab unit cell.

3.2. Electronic properties of TaON bulk

Using meta-GGA, the band structures and DOS/PDOS are calculated from the optimized crystal structures and shown in Fig. 2. The DOS of TaON bulk in the energy region between −10 and +10 eV is given in Fig. 3 where the Fermi energy (4.60 eV) is set to zero. The occupied Ta 5d band is lower in energy than to the N 2p and O 2p bands, resulting in an N 2p valence band and Ta 5d conduction band with a band gap of 2.44 eV.

Considering the PDOS of TaON, the top of valence band (VB) mainly consists of bonding N 2p states along with some contribution from O 2p states and a minor contribution from the bonding, Ta 5d states (Fig. 2). These orbitals of N 2p, O 2p, and Ta 5d states lead to a strong hybridization which respectively occupy the upper and lower part of the valence band, form the bonding states in this energy region. The middle of the VB contains Ta 5d hybridized with N and O 2p while the lowest energy edge of the VB has an increased contribution from O 2p mixed

with N 2p (Fig. 2). The CB of TaON bulk is mainly composed of the anti-bonding Ta 5d states along with a minor contribution from O and N 2p states. In this regard, the anti-bonding states in the conduction band of TaON is almost (totally) constituted by the electronic states of Ta atoms. Moreover, from the PDOS of TaON, it can be analyzed that there is no hybridization between the orbitals of these three different atoms in its conduction band region (Fig. 2a). The lower region of the CB is equally contributed by the 2p states of O and N which evidences their strong overlapping in form of hybridization.

To understand the individual fundamental electronic structure of the occupied and unoccupied states, within the VB and CB of TaON; they are given in Fig S1. From Fig S1 and Scheme S1, the contribution of N, O, and Ta both in the VB and CB can be clearly visualized.

Band structures of the primitive unit cell and supercell (bulk) of TaON are given in Fig S2 and Fig. 3, respectively. TaON has an indirect band gap (2.42 eV) which changes to direct (2.44 eV), considering the supercell ($2 \times 2 \times 2$) as can be seen from its band structure (Fig. 3). This band gap changes from the indirect to direct is because of the geometric change, as the computational settings are effectively different in these two calculations.

The theoretical band gap is also checked from the DOS plot as given in Fig. 2a. The direct band gap is due to the electronic excitation of an electron from the $\Gamma \rightarrow \Gamma$. More clearly, a direct band gap is characterized by having the band edges aligned in the similar k-space so, that an electron can transit from the valence to the conduction band, with the emission of a photon, without changing considerably the momentum. On the other hand, in the indirect band gap, the band edges are not aligned so, the electron does not transit directly to the conduction band where both photon and phonon are involved. At the Fermi energy of 4.60 eV, the vacuum phase VBM and CBM values are ca. −6.54 and −4.10 eV, respectively. Both the VBM and CBM are well below and above the redox potential of water (Scheme 1). Moreover, our computed band gap (2.44 eV) has nice correlation with that of the experimental (~2.40 eV) [28,45]. Furthermore, our simulated Fermi energy, VB and CB has also excellent correlation with the experimental work of Chun et al. [28], where the Fermi energy level is −4.41 eV, VB −6.45 eV and CB −4.10 eV (see Table 1). This nice correlation between the experimental and our theoretical data validate and confirm the method used.
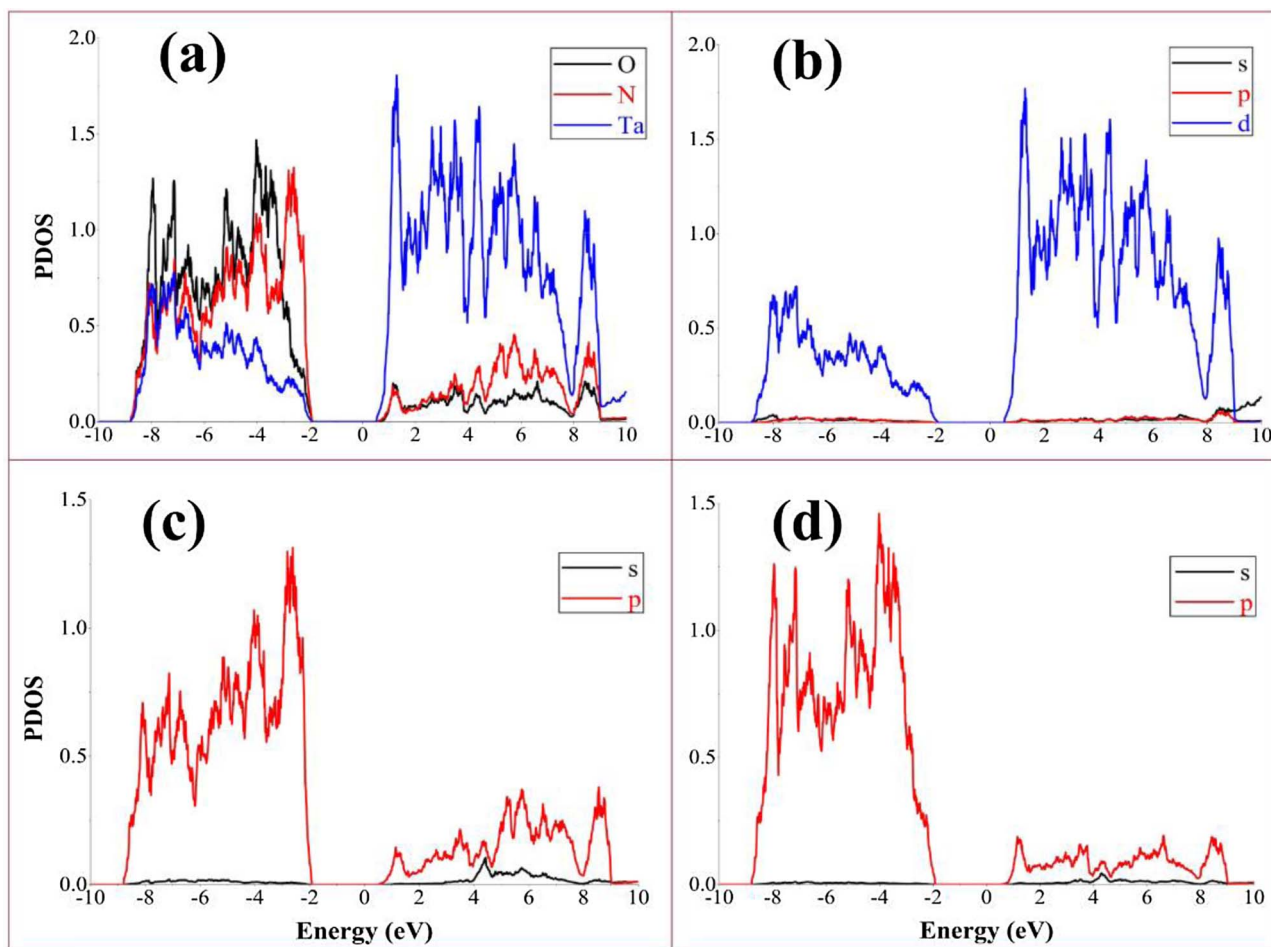
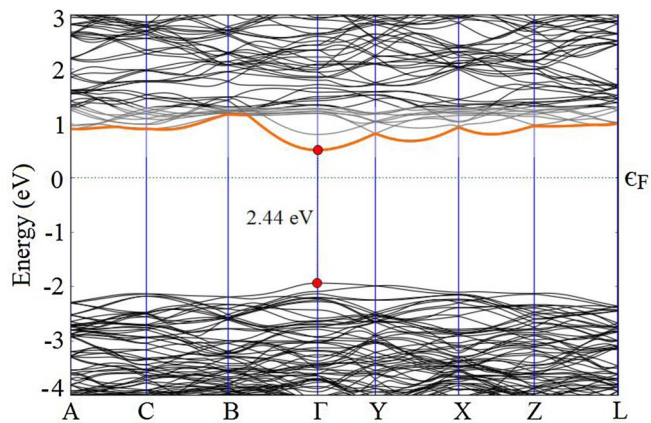**Fig. 2.** PDOS of TaON bulk (a), Ta (b), N (c), and O PDOS (d); the Fermi Energy is set to zero.

Fig. 3. Band Structure of the $2 \times 2 \times 2$ supercell of TaON; the Fermi Energy is set to zero.

3.3. Electronic and optical properties N terminated TaON(001) surface

The simulated PDOS of the N terminated TaON(001) surface is given in Fig. 4, where the VBM and CBM positions are located at -0.61 and $+1.50$ eV, respectively. The Fermi energy is set to zero which is 5.16 eV. The occupied band (-7.0 to -0.61 eV) which lie below the Fermi energy level is dominated by the 2p orbitals of N along with an equal contribution from 5d of Ta and 2p of O atoms (Fig. 4a). While its CBM is dominated by 5d of Ta with no contribution from either O or N orbitals. In case of water interacted systems; the VBM is constituted by N 2p and with an equal hybridized contribution of Ta 5d and O 2p orbitals. Again, the CBM is made of Ta atom but at a higher potential (2.46 eV compared to 1.50 eV) and with minor contribution of anti-bonding orbitals of O and N atoms (Fig. 4b). Hydrogen of water has slight contribution in the lower energy region of VBM as can be seen from Fig. 4b. At vacuum phase, the VBM and CBM of N terminated TaON(001) are situated ca. -5.77 and -3.66 eV, respectively (Table 1).

Table 1
Fermi Energy level, VBM, and CBM at vacuum level, Band Gap (in unit of eV), Effective Masses of Photogenerated Electrons and Holes; Estimated from the calculated Band Structure along the suitable direction.

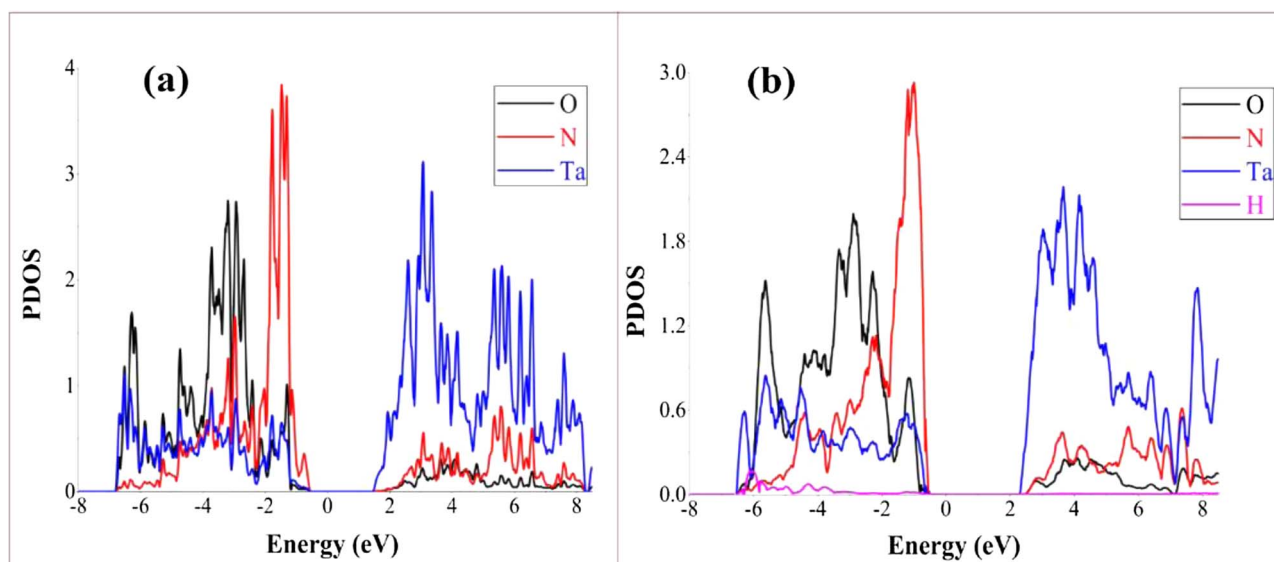| Species	Surface atoms	Fermi level	m_e^*/m_0 (m_e)	m_h^*/m_0 (m_e)	VBM	CBM	Band gap
TaON	Bulk	-4.60	0.85	0.82	-6.54	-4.10	2.44
TaON(001)	N*	-5.16	0.81	3.99	-5.77	-3.66	2.11
TaON(001)@H$_2$O	~	-5.01	1.49	3.46	-5.64	-2.55	3.09
TaON(010)	O	-5.78	0.67	1.63	-6.36	-3.34	3.02
TaON(010)@H$_2$O	~	-4.83	0.72	1.64	-5.42	-2.24	3.18

Fig. 4. PDOS of N_TaON(001), (a) and N_TaON(001)@H$_2$O, (b); the Fermi energy is set to zero.
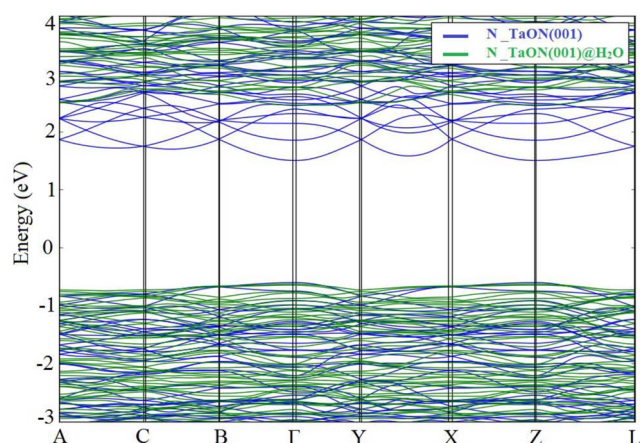

Fig. 5. Comparative band structures of N terminated TaON(001) and TaON(001)@H$_2$O; Fermi Energy is set to zero.

The simulated band structure of pristine N terminated TaON(001) is given in Fig. 5, having band gap of 2.11 eV. Upon adsorption of water molecule, its band gap elongates to 3.09 eV which is due to the reduction nature of H$_2$O. This band gap difference of 0.98 eV is because of the shifting of CBM towards more positive potential (2.46 eV) as can be seen from Figs. 4 and 5. The effective mass of photogenerated electrons and holes is an important parameter which determines the charge recombination rate. The quantum efficiency of a photocatalytic reaction is directly dependent on the relative transfer rate of photogenerated electrons to holes and whether these recombine or dissociate. When light irradiates on a photoactive material, it generates coulombically bound electron–hole pairs. The transfer rate of the photogenerated electrons and holes can be directly evaluated from their effective masses, using Eq. (2).

$$v = k/m^* \qquad (2)$$

where m^* represent the effective mass of charge carrier, k is the wave vector and v is the transfer rate of photogenerated electrons and holes.

To investigate the photocatalytic activity of TaON, the effective mass of electrons (m_e^*) and holes (m_h^*) along the appropriate directions k-points are calculated by fitting parabolas on a 1 meV region for the bottom of the CBM or the top of the VBM, respectively and using Eq. (3):

$$m^* = \hbar^2 \, (\mathrm{d}^2 \, E/\mathrm{d}k^2)^{-1} \qquad (3)$$

where $\hbar$ is the reduced Planck constant, E is the energy of an electron at wave vector k in the same band (VBM or CBM). The estimated effective masses of electrons and holes for the different systems considered in this paper are listed in Table 1.

The adsorption of water molecule is non-dissociative where H of water interacts with the N and O of TaON(001) slab. The adsorption energy of these non-covalent bondings is about -118 kJ mol^{-1} (Table 2). The water adsorption energies were calculated by subtracting the energies of the optimized water molecule and adsorbent bare slab (E_{slab}) from the optimized water-slab complex (slab@water), using Eq. (4).

$$\Delta E_{ad} = E_{slab@water} - (E_{water} + E_{slab}) \qquad (4)$$

As we know, these photogenerated electrons and holes thermally relax to the bottom of the conduction band and the top of the valence band, respectively so, that is why these regions are considered. The simulated values of the effective masses of photogenerated electrons and holes for the N_TaON(001) are 0.81 and 3.99 m_e, respectively. On interaction with H$_2$O molecule the effective mass of electrons and holes change to 1.49 and 3.46 m_e, respectively.

To further elaborate the interaction of water molecule on the N terminated TaON(001) surface, UV–vis absorption spectra are simulated which is given in Fig. 6. Pristine N_TaON(001) give rise to λ_{max} of 442 nm which became blue shifted (367 nm) when water is adsorbed. In summary, N_TaON(001) surface has good interaction ability towards H$_2$O besides its non-suitable VBM position (-5.77 eV vs vacuum). However, it can absorb the visible part of solar irradiation as can be seen from Fig. 6. The water adsorption over N_TaON(001) surface can also be visualized from its electron localization plot (Fig. 7).

3.4. Electronic and optical properties O terminated TaON(010) surface

The PDOS of O terminated TaON(010) is given in Fig. 8a, where the VBM and CBM are located at -0.58 and 2.44 eV, respectively (at Fermi

Table 2
Adsorption Energy of Water with the N and O terminated surfaces of TaON.

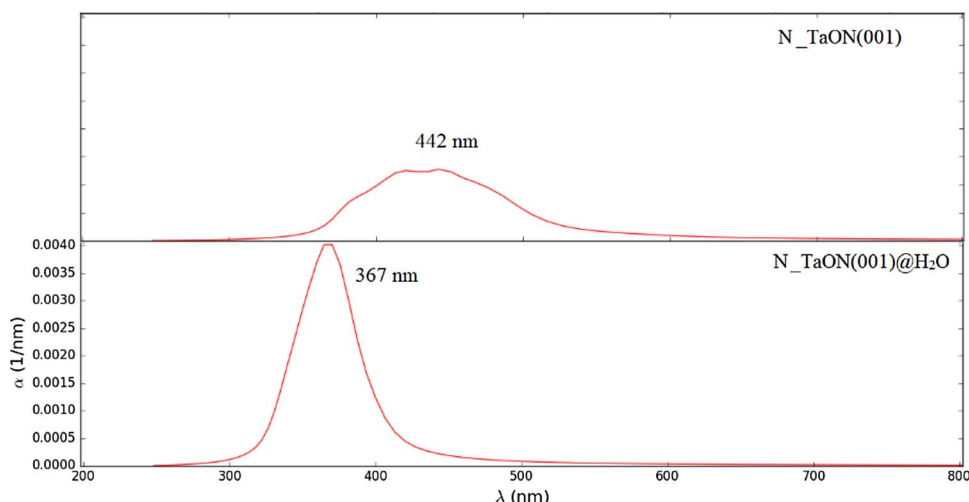| Species	Surface atoms	Adsorption Energy (kJ/mol)
TaON(001)@H$_2$O	N	-118
TaON(010)@H$_2$O	O	-148

Fig. 6. UV–vis absorption spectra of N terminated TaON(001) and TaON(001)@H₂O.
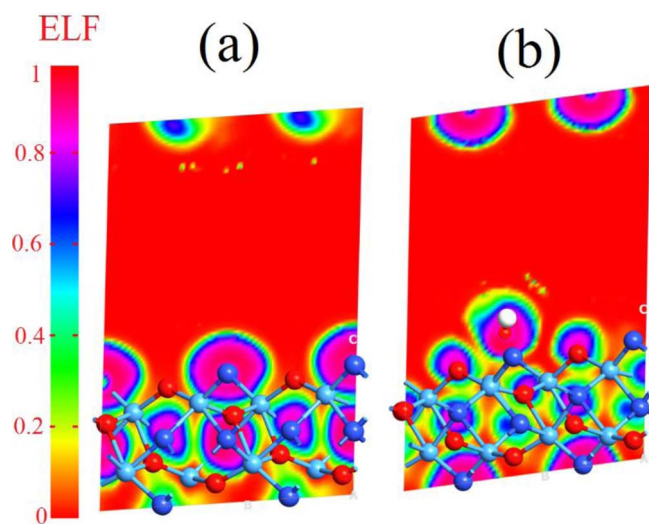

Fig. 7. Electron localization function map of (a) N_TaON(001) and (b) N_TaON(001)@H₂O.

energy of 5.78 eV). The PDOS of O_TaON(010) depicts that the VBM is located at −0.58 eV (−6.36 eV vs vacuum), having major contribution of N 2p along with minor participation of Ta 5d, and O 2p orbitals (Fig. 8a).) This behaviour is consistent with its respective bulk. The

electronic states of unoccupied band of O_TaON(010) are calculated in the range, +2.44 to +10 eV, where the CB edge is constituted by the anti-bonding orbitals of Ta 5d, along with almost no contribution of N 2p and O 2p orbitals. The whole CB of O_TaON(010) is uniformly made from the anti-bonding orbitals of Ta 5d and is situated (−3.34 eV vs vacuum) at well above the redox CBM level of water (Scheme 1). The bottom section of CB is equally contributed by the hybridized orbitals of 2p of N and O (Fig. 8a). On adsorption of water molecule, the CBM move towards more positive potential which results a wide band gap compared to parent slab (Fig. 8b).

The CBM of O_TaON(010) moved from 2.44 to 2.59 eV when water molecule is adsorbed on its surface, as can be clearly seen from their comparative band structures (Fig. 9). Analysis of Figs. 8 and 9 led us to conclude that the band gap of O_TaON(010) increases from 3.02 to 3.18 eV upon adsorption of H₂O. Furthermore, to check the photo-catalytic efficiency of this surface, effective masses of photogenerated electrons and holes are estimated from its band structure. The effective masses of electrons and holes of parent O_TaON(010) are 0.67 and 1.63 m_e, respectively which increase when water is adsorbed, as can be seen from Table 1.

As discussed earlier, O_TaON(010) surface has an ideal VBM and CBM positions along with small effective masses of election and hole. However, due to its large band gap (3.01 eV) it cannot easily absorb the visible part of sun light as can be seen from its UV spectra (Fig. 10). A blue-shifting in λ_{max} is observed when H₂O is presents on the surface of O_TaON(010). Water molecule has shifted the λ_{max} of O_TaON(010)
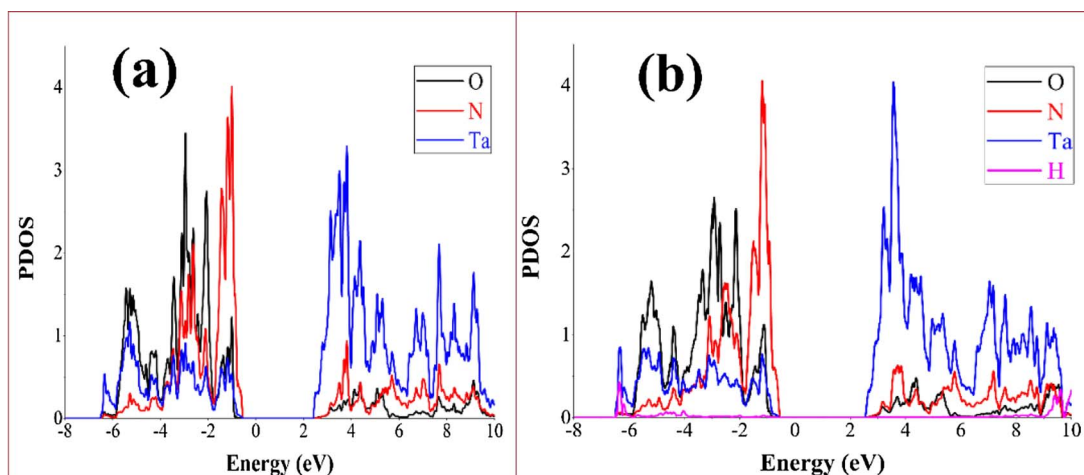

Fig. 8. PDOS of O_TaON(010), (a) and O_TaON(010)@H₂O, (b); Fermi energy is set to zero.
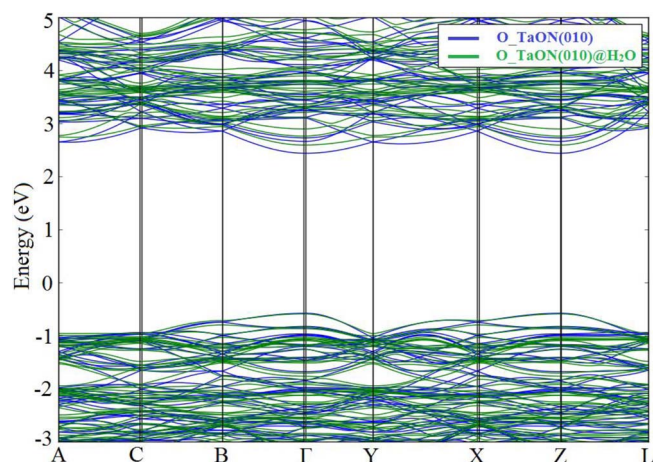
Fig. 9. Comparative band structure of O terminated TaON(010) and TaON(010)@H₂O; Fermi energy is set to zero.

Fig. 11. Electron localization function map of O_TaON(010) and O_TaON(010)@H₂O.

from 368 to 332 nm which consequences its good adsorption capability. Moreover, this shifting in λ_{max} (36 nm) strongly corroborates the previous characterizations such as effective masses of charge carriers and VBM and CBM positions.

An adsorption energy of $-148\,kJ\,mol^{-1}$ is observed between water molecule and O_TaON(010) surface. This non-dissociative high adsorption is because of H of water and O of slab along with contribution from the O of water and N of slab. Furthermore, this non-covalent interaction can also be seen from the electron localization function plots, given in Fig. 11.

4. Conclusion

Periodic density functional theory calculations for bulk and potential photoelectrode thin films of β-TaON are carried out considering N, Ta, and O terminations. We investigate their electronic and optical properties and photocarrier mobility. Firstly, the electronic properties of bulk β-TaON predict TaON is a better candidate for photocatalytic water splitting than either Ta_2O_5 or Ta_3N_5. The DOS and PDOS
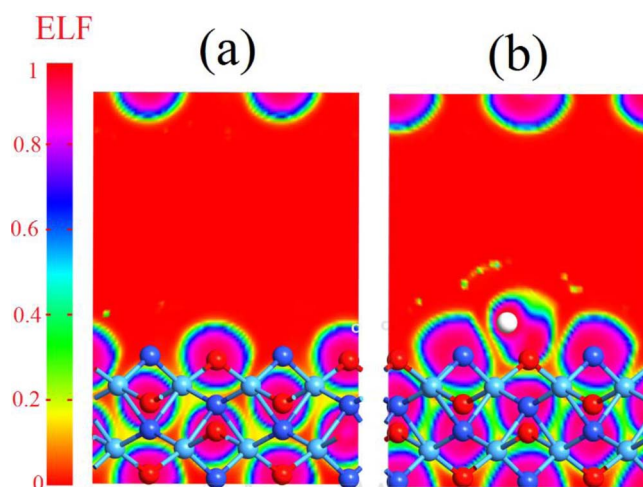
simulation predict that valence band of all these studied systems is constituted by the 2p orbitals of N with a minor contribution of O 2p, while anti-bonding orbitals of 5d of Ta are responsible for the conduction band. We have simulated the effective masses of the photo-generated electrons and hole for the mentioned species. The large difference in the effective masses of electrons and hole are found which is a direct consequence of high charge dissociation instead of recombination. In summary, the oxygen and nitrogen terminated TaON along (010) and (001), respectively has good stability and sensitivity towards water molecule. Moreover, O terminated TaON has ideal band edge positions while N terminated has strong ability towards visible light absorption, so a mixed phase would result an efficient photoanode for water splitting. Furthermore, the development of effective dopants will be very crucial in improving the transport properties of the surface of TaON to further reduce the masses of photogenerated electrons and holes for high charge mobility rate.
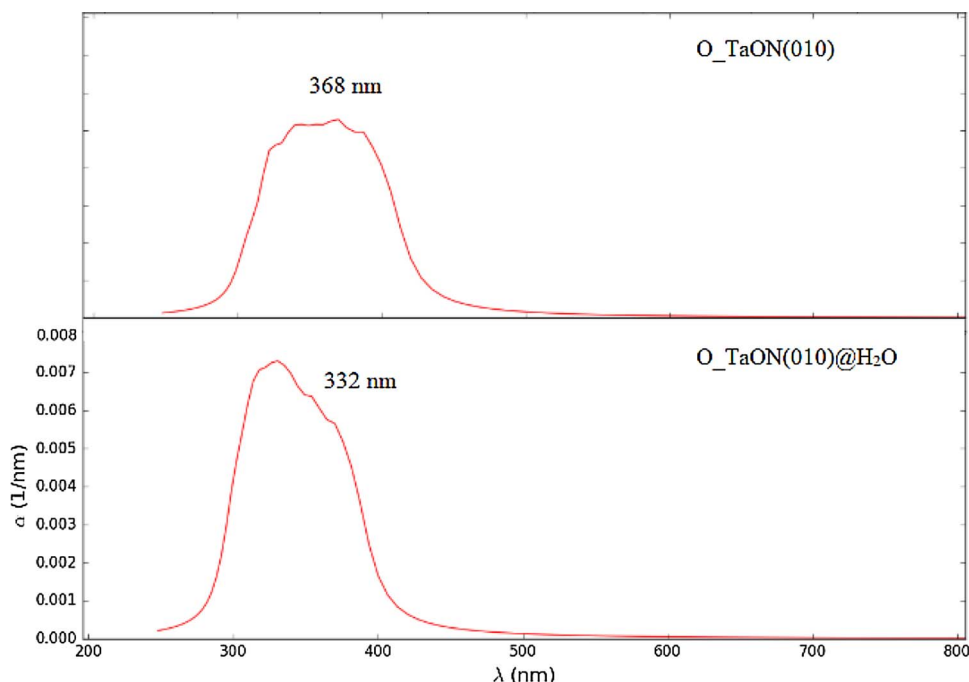

Fig. 10. UV–vis absorption spectra of O terminated TaON(010) and TaON(010)@H₂O.

Appendix A. Supplementary data

Table of crystallographic and simulated parameters, Schematic representation of VB and CB of TaON, band structure, and electron difference density plots of N_, and O_TaON(010) along with water adsorbed systems are given in the supporting information.

Supplementary material related to this article can be found, in the online version, at doi:https://doi.org/10.1016/j.apcatb.2018.02.001.

References

[1] Y. Tachibana, L. Vayssieres, J.R. Durrant, Artificial photosynthesis for solar water-splitting, Nat. Photon. 6 (2012) 511–518.

[2] A.M. Hafez, A.F. Zedan, S.Y. AlQaradawi, N.M. Salem, N.K. Allam, Computational study on oxynitride perovskites for CO 2 photoreduction, Energy Convers. Manage. 122 (2016) 207–214.

[3] S.W. Boettcher, T.E. Mallouk, F.E. Osterloh, Themed issue on water splitting and photocatalysis, J. Mater. Chem. A 4 (2016) 2764–2765.

[4] S. Giménez, J. Bisquert, Photoelectrochemical Solar Fuel Production: From Basic Principles to Advanced Devices, Springer, 2016.

[5] A. Fujishima, K. Honda, Photolysis-decomposition of water at the surface of an ir-radiated semiconductor, Nature 238 (1972) 37–38.

[6] S. Sonoda, O. Kawasaki, J. Kato, M. Takenaga, Photocatalyst material and photo-catalyst device, (2016) US Patent 20,160,093,448.

[7] M. Fujihara, Introduction—solar to chemical energy conversion, Solar to Chemical Energy Conversion, Springer, 2016, pp. 1–3.

[8] J. Li, N. Wu, Semiconductor-based photocatalysts and photoelectrochemical cells for solar fuel generation: a review, Catal. Sci. Technol. 5 (2015) 1360–1384.

[9] R. Abe, M. Higashi, K. Domen, Facile fabrication of an efficient oxynitride TaON photoanode for overall water splitting into H2 and O2 under visible light irradia-tion, J. Am. Chem. Soc. 132 (2010) 11828–11829.

[10] C. Pan, T. Takata, M. Nakabayashi, T. Matsumoto, N. Shibata, Y. Ikuhara, K. Domen, A complex perovskite-type oxynitride: the first photocatalyst for water splitting operable at up to 600 nm, Angew. Chem. Int. Ed. 54 (2015) 2955–2959.

[11] J. Xu, C. Pan, T. Takata, K. Domen, Photocatalytic overall water splitting on the perovskite-type transition metal oxynitride CaTaO 2 N under visible light irradia-tion, Chem. Commun. 51 (2015) 7191–7194.

[12] C. Pan, T. Takata, M. Nakabayashi, T. Matsumoto, N. Shibata, Y. Ikuhara, K. Domen, Innentitelbild: a complex perovskite-type oxynitride: the first photo-catalyst for water splitting operable at up to 600 nm (Angew. Chem. 10/2015), Angew. Chem. 127 (2015) 2900.

[13] T. Takata, C. Pan, K. Domen, Recent progress in oxynitride photocatalysts for visible-light-driven water splitting, Sci. Technol. Adv. Mater. 16 (2015) 1468–6996.

[14] C. Pan, T. Takata, K. Domen, Overall water splitting on the transition-metal oxy-nitride photocatalyst LaMg1/3Ta2/3O2N over a large portion of the visible-light spectrum, Chem.-Eur. J. 22 (2016) 1854–1862.

[15] S. Landsmann, A.E. Maegli, M. Trottmann, C. Battaglia, A. Weidenkaff, S. Pokrant, Design guidelines for high-performance particle-based photoanodes for water splitting: lanthanum titanium oxynitride as a model, ChemSusChem 8 (2015) 3451–3458.

[16] C. Zhen, R. Chen, L. Wang, G. Liu, H.-M. Cheng, Tantalum (oxy) nitride based photoanodes for solar-driven water oxidation, J. Mater. Chem. A 4 (2016) 2783–2800.

[17] S.S. Gujral, A.N. Simonov, M. Higashi, X.-Y. Fang, R. Abe, L. Spiccia, Highly dis-persed cobalt oxide on TaON as efficient photoanodes for long-term solar water splitting, ACS Catal. 6 (2016) 3404–3417.

[18] Z. Zhao, Z. Wang, J. Bao, Nanomaterials for hydrogen generation from solar water splitting, Nanomaterials for Sustainable Energy, Springer, 2016, pp. 445–470.

[19] G. Hitoki, T. Takata, J.N. Kondo, M. Hara, H. Kobayashi, K. Domen, An oxynitride, TaON, as an efficient water oxidation photocatalyst under visible light irradiation (λ ≤ 500 nm), Chem. Commun. (2002) 1698–1699.

[20] T. Lüdtke, A. Schmidt, C. Göbel, A. Fischer, N. Becker, C. Reimann, T. Bredow, R. Dronskowski, M. Lerch, Synthesis and crystal structure of δ-TaON, a metastable polymorph of tantalum oxide nitride, Inorg. Chem. 53 (2014) 11691–11698.

[21] M. de Respinis, M. Fravventura, F.F. Abdi, H. Schreuders, T.J. Savenije, W.A. Smith, B. Dam, R. van de Krol, Oxynitrogenography: controlled synthesis of single-phase tantalum oxynitride photoabsorbers, Chem. Mater. 27 (2015) 7091–7099.

[22] N.K. Allam, B.S. Shaheen, A.M. Hafez, Layered tantalum oxynitride nanorod array carpets for efficient photoelectrochemical conversion of solar energy: experimental and DFT insights, ACS Appl. Mater. Interfaces 6 (2014) 4609–4615.

[23] S. Balaz, S.H. Porter, P.M. Woodward, L.J. Brillson, Electronic structure of tantalum oxynitride perovskite photocatalysts, Chem. Mater. 25 (2013) 3337–3343.

[24] R. Sasaki, K. Maeda, Y. Kako, K. Domen, Preparation of calcium tantalum oxynitride from layered oxide precursors to improve photocatalytic activity for hydrogen evolution under visible light, Appl. Catal. B: Environ. 128 (2012) 72–76.

[25] Z.-H. Cui, H. Jiang, Theoretical investigation of Ta2O5, TaON, and Ta3N5: elec-tronic band structures and absolute band edges, J. Phys. Chem. C 121 (2017) 3241–3251.

[26] M. de Respinis, M. Fravventura, F.F. Abdi, H. Schreuders, T.J. Savenije, W.A. Smith, B. Dam, R. van de Krol, Oxynitrogenography: controlled synthesis of single-phase tantalum oxynitride photoabsorbers, Chem. Mater. 27 (2015) 7091–7099.

[27] P. Carvalho, J. Borges, M. Rodrigues, N. Barradas, E. Alves, J. Espinós, A. González-Elipe, L. Cunha, L. Marques, M. Vasilevskiy, Optical properties of zirconium oxy-nitride films: the effect of composition, electronic and crystalline structures, Appl. Surf. Sci. 358 (2015) 660–669.

[28] W.-J. Chun, A. Ishikawa, H. Fujisawa, T. Takata, J.N. Kondo, M. Hara, M. Kawai, Y. Matsumoto, K. Domen, Conduction and valence band positions of Ta2O5, TaON, and Ta3N5 by UPS and electrochemical methods, J. Phys. Chem. B 107 (2003) 1798–1803.

[29] C. Taviot-Guého, J. Cellier, A. Bousquet, E. Tomasella, Multiphase structure of tantalum oxynitride TaO x N y thin films deposited by reactive magnetron sput-tering, J. Phys. Chem. C 119 (2015) 23559–23571.

[30] H. Wolff, T. Bredow, M. Lerch, H. Schilling, E. Irran, A. Stork, R. Dronskowski, A first-principles study of the electronic and structural properties of γ-TaON, J. Phys. Chem. A 111 (2007) 2745–2749.

[31] H. Schilling, A. Stork, E. Irran, H. Wolff, T. Bredow, R. Dronskowski, M. Lerch, γ-TaON: a metastable polymorph of tantalum oxynitride, Angew. Chem. Inter. Ed. 46 (2007) 2931–2934.

[32] M.W. Lumey, R. Dronskowski, The electronic structure of tantalum oxynitride and the falsification of α-TaON, Zeitschrift für anorganische und allgemeine Chemie 629 (2003) 2173–2179.

[33] S. Yoon, A.E. Maegli, S.K. Matam, M. Trottmann, T. Hisatomi, C.M. Leroy, M. Grätzel, S. Pokrant, A. Weidenkaff, The influence of the ammonolysis tem-perature on the photocatalytic activity of β-TaON, Int. J. Photoenergy 2013 (2013).

[34] G. Brauer, J. Weidlein, Synthesis and properties of tantalum oxide nitride, TaON, Angew. Chem. Inter. Ed. 4 (1965) 875.

[35] P. Giannozzi, S. Baroni, N. Bonini, M. Calandra, R. Car, C. Cavazzoni, D. Ceresoli, G.L. Chiarotti, M. Cococcioni, I. Dabo, QUANTUM ESPRESSO: a modular and open-source software project for quantum simulations of materials, Phys. Condens. Matt. 21 (2009) 395502.

[36] AtomistixToolKit, version 2017.1, QuantumWise A/S, (www.quantumwise.com).

[37] VirtualNanoLab, version 2017.1, QuantumWise A/S, (www.quantumwise.com).

[38] D. Armytage, B. Fender, Anion ordering in NaON: a powder neutron-diffraction investigation, Acta Crystallogr. Sect. B: Crystallogr. Cryst. Chem. 30 (1974) 809–812.

[39] A.H. Larsen, M. Vanin, J.J. Mortensen, K.S. Thygesen, K.W. Jacobsen, Localized atomic basis set in the projector augmented wave method, Phys. Rev. B 80 (2009) 195112.

[40] G. Kresse, D. Joubert, From ultrasoft pseudopotentials to the projector augmented-wave method, Phys. Rev. B 59 (1999) 1758.

[41] R. Peverati, D.G. Truhlar, Improving the accuracy of hybrid meta-GGA density functionals by range separation, J. Phys. Chem Lett. 2 (2011) 2810–2817.

[42] J. Hafner, Materials simulations using VASP—a quantum perspective to materials science, Comput. Phys. Commun. 177 (2007) 6–13.

[43] J. Endres, D.A. Egger, M. Kulbak, R.A. Kerner, L. Zhao, S.H. Silver, G. Hodes, B.P. Rand, D. Cahen, L. Kronik, Valence and conduction band densities of states of metal halide perovskites: a combined experimental–theoretical study, J. Phys. Chem. Lett. 7 (2016) 2722–2729.

[44] C. Kittel, Introduction to Solid State Physics, Wiley, 2005.

[45] T.K. Ghosh, N.N. Nair, Nature of β-TaON surfaces at ambient conditions, Surf. Sci. 635 (2015) 19–26.